$LaCrSb_3$: A New Itinerant Electron Ferromagnet with a Layered Structure

N. P. Raju and John E. Greedan*

Brockhouse Institute for Materials Research, McMaster University, Hamilton, ON, Canada L8S 4M1

Michael J. Ferguson and Arthur Mar*

Department of Chemistry, University of Alberta, Edmonton, AB, Canada T6G 2G2

Received May 27, 1998. Revised Manuscript Received August 12, 1998

$LaCrSb_3$, a new layered material, crystallizes in space group *Pbcm* with $a = 13.266(3)$, $b = 6.188(1)$, and $c = 6.100(1)$ Å at 293 K as determined by neutron diffraction. Corrugated $CrSb_2$ layers are stacked normal to [100] and are separated by La^{3+} ions and a nearly square planar Sb layer. Resistivity data indicate metallic behavior parallel to the *c*-axis. At low temperatures, the resistivity follows a T^2 law with an inflection point at about 125 K, above which a weaker temperature dependence is seen. Magnetization measurements also indicate a phase transition at 125 K of apparently ferromagnetic nature. A saturation moment of 0.8 μ_B is derived at 5 K, and a decidedly non-Curie−Weiss temperature dependence is obtained between 125 and 700 K. Neutron diffraction data verify the ferromagnetic structure at zero applied field with a moment of 0.79(3) μ_B/Cr and a moment direction [010]. The temperature dependence of the unit cell constants is highly anisotropic with the *c*-axis displaying an anomaly at T_c. These properties are indicative of itinerant electron ferromagnetic behavior arising from strong electron correlation in the Cr d-bands. Band structure calculations in the extended Hückel approximation support a highly two-dimensional electronic structure comprised of contributions from Cr−Sb and Sb−Sb layers that interact very weakly along the stacking direction, *a**. The Fermi level is found near a DOS maximum composed largely of Cr d-bands, but there is considerable Cr−Sb d−p mixing.

Introduction

$LaCrSb_3$ is a member of a newly discovered series of compounds, $RECrSb_3$ with RE = La, Ce, Pr, Nd, Sm, Gd, Tb, and Dy, with a structure consisting of anionic $CrSb_2$ layers built up from face- and edge-sharing $CrSb_6$ octahedra and anionic square nets of Sb, both separated by La cations (Figure 1).[1,2] The space group is *Pbcm*, and for RE = La, $a = 13.2835(7)$, $b = 6.2127(2)$, and $c = 6.116(1)$ Å at room temperature.[1] The $CrSb_2$ layers are stacked normal to the [100] direction, and the nearest Cr−Cr interlayer distance is 11.31 Å.[1] The Cr−Sb distances (2.698(4)−2.747(3) Å)[1] are consistent with a formal Cr oxidation state between +3 (found in CrSb, 2.745 Å)[3] and +4 (found in $CrSb_2$, 2.708(1) Å).[4] These observations suggest that the physical properties of the $RECrSb_3$ materials might be interesting. We report here the first measurements of the electronic properties of any member of this series beginning with $LaCrSb_3$.

Experimental Section

Synthesis. Bulk phase samples of $LaCrSb_3$ for neutron diffraction and magnetic susceptibility measurements were prepared from powders of the elements (La, 99.9%, Alfa-Aesar; Cr, 99.95%, Cerac; Sb, 99.995%, Aldrich). The elements were loaded into fused-silica tubes (5 cm length, 10 mm i.d.) in a 1:1:3 ratio, which were then evacuated, sealed, and heated in

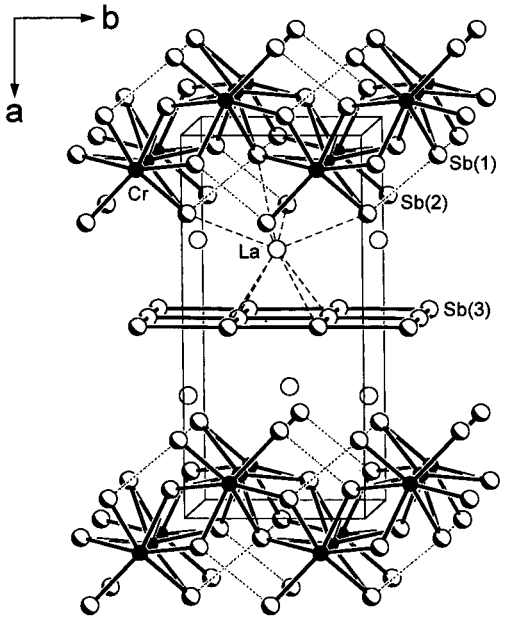

Figure 1. Crystal structure of $LaCrSb_3$. Note that the layers of Cr−Sb face- and edge-sharing octahedra and square Sb nets are stacked along the *a*-axis.

(1) Ferguson, M. J.; Hushagen, R. W.; Mar, A. *J. Alloys Compd.* **1997**, *249*, 191.
(2) Brylak, M.; Jeitschko, W. *Z. Naturforsch. B: Chem. Sci.* **1995**, *50*, 899.
(3) Kjekshus, A.; Walseth, K. P. *Acta Chem. Scand.* **1969**, *23*, 2621.
(4) Holseth, H.; Kjekshus, A. *Acta Chem. Scand.* **1968**, *22*, 3284.

10.1021/cm9803758 CCC: $15.00
Published on Web 10/10/1998

Table 1. Profile Refinements Results for $LaCrSb_3$, 5 and 150 K

	5 K			150 K		
space group		*Pbcm*			*Pbcm*	
a (Å)		13.264(3)			13.264(3)	
b (Å)		6.182(2)			6.186(1)	
c (Å)		6.094(2)			6.099(1)	
	x	*y*	*z*	*x*	*y*	*z*
La	0.3229(10)	0.0130(42)	1/4	0.3213(9)	0.0149(37)	1/4
Cr	0.9253(32)	1/4	0	0.9266(28)	1/4	0
Sb(1)	0.0662(19)	0.0787(39)	1/4	0.0681(17)	0.0809(35)	1/4
Sb(2)	0.2240(13)	0.5284(70)	1/4	0.2250(12)	0.5220(64)	1/4
Sb(3)	0.4856(31)	1/4	0	0.4883(29)	1/4	0
B(overall) (Å^2)		5.3(9)			3.8(7)	
R_{wp} (%)		4.94			4.58	
R_E (%)		2.50			1.36	
Cr moment (μ_B)		0.79(3)				
moment direction		[010]				
R_{mag} (%)		14.3				

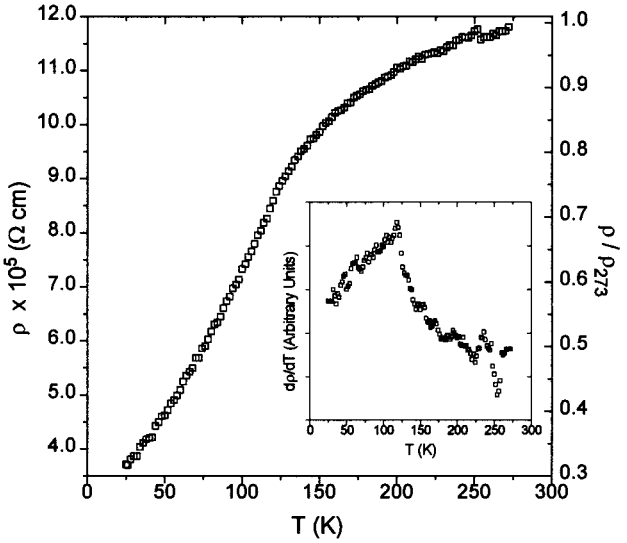

Figure 2. Resistivity of a single crystal of $LaCrSb_3$ measured parallel to the *c*-axis. The inset shows the temperature dependence of dρ/dT.

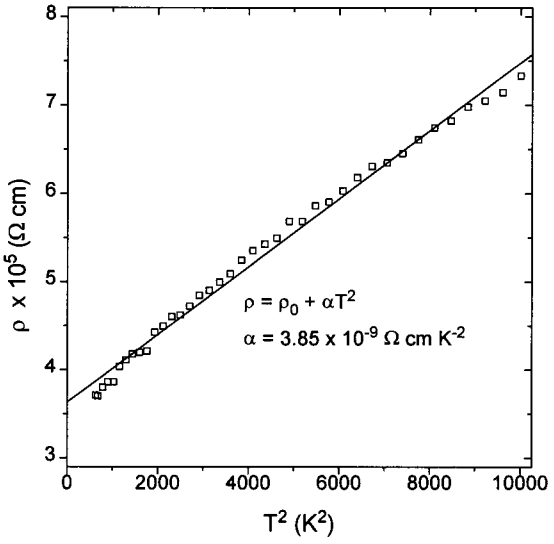

Figure 3. Fit of the low-temperature resistivity data of $LaCrSb_3$ to $\rho = \rho_0 + \alpha T^2$.

a furnace. The tubes were typically heated at 570 °C for 1 day and 1000 °C for 3 days and then cooled to 20 °C over 2−4 days. The samples were analyzed by their powder X-ray diffraction patterns collected on an Enraf-Nonius FR552 Guinier camera (Si standard). The ternary compound was identified as the major phase with only minor amounts (<10%) of Sb impurity.

Table 2. Extended Hückel Parameters

atom	orbital	H_{ii} (eV)	ξ_{i1}	c_1	ξ_{i2}	c_2
La	6s	−6.5613	2.14			
	6p	−4.3769	2.08			
	5d	−7.5155	3.78	0.77651	1.381	0.45861
Cr	4s	−8.66	1.7			
	4p	−5.24	1.7			
	3d	−11.22	4.95	0.5060	1.80	0.6750
Sb	5s	−18.8	2.323			
	5p	−11.7	1.999			

Single crystals of $LaCrSb_3$ used for the resistivity measurements were prepared as above, with a slightly different temperature program. The tubes were heated at 570 °C for 1 day and 1000 °C for 3 days and then slowly cooled to 20 °C over 8 days. Single crystals with a tabular habit and up to 1 mm in length were extracted from the reaction mixture, which also contains other binary phases. Elemental composition of the selected crystals was verified by EDX (energy-dispersive X-ray) analysis on a Hitachi F2700 scanning electron microscope.

Electrical Resistivity. The same crystals that were analyzed on the SEM were used for the resistivity measurements. Four Au wires with graphite extensions were attached with Ag paint to crystals with lengths between 0.7 and 1.0 mm for the four-probe ac resistivity technique at 15.9 Hz. Data were collected on cooling and warming between 20 and 300 K.

Magnetic Susceptibility. Magnetic data were collected on a SQUID magnetometer (Quantum Design) at various applied fields (0.01−5 T) and over the temperature range 5−700 K.

Neutron Diffraction. Neutron diffraction data were collected on the C2 instrument of the DUALSPEC installation at the Chalk River Nuclear Laboratories and the Neutron Program for Materials of the National Research Council of Canada. The neutron wavelength was 2.3692 Å. The polycrystalline sample was contained in a vanadium can sealed under helium exchange gas with an indium gasket and attached to the cold stage of a liquid helium cryostat. Temperature control was to within ±0.1 K. Analysis of the neutron diffraction data was carried out using either DBWS PC96005[5] or FULLPROF version 3.5.[6] Results from the profile refinements of the 5 and 150 K data are collected in Table 1.

(5) Wiles, D. B.; Young, R. A. *J. Appl. Crystallogr.* **1981**, *14*, 149.
(6) Rodriguez-Carvajal, J. *FULLPROF: A Program for Rietveld Refinement and Profile Matching Analysis*; Laboratoire Leon Brillouin (CEA-CNRS): Saclay, France. For information on version 3.5 contact J. Rodriguez-Carvajal: (fax (33) 1 6908 8261; e-mail juan@bali.saclay.fr).

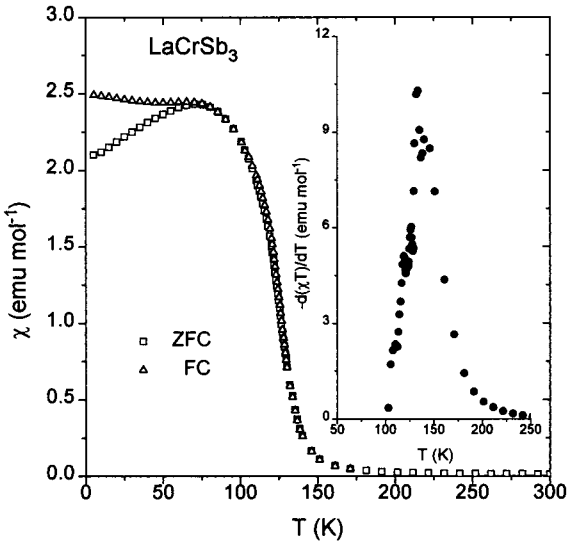

Figure 4. Susceptibility of $LaCrSb_3$ as a function of temperature at an applied field of 0.01 T. The inset shows the function $-d(\chi T)/dT$ versus temperature.

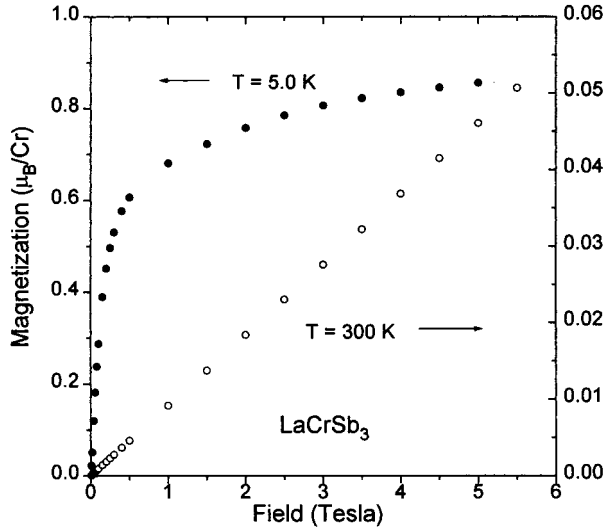

Figure 5. Isothermal magnetization of $LaCrSb_3$ at 5 and 300 K.

Band Structure. One-electron band structure calculations on the room-temperature structure of $LaCrSb_3$ were performed by the tight-binding method with an extended Hückel-type Hamiltonian using the EHMACC suite of programs.[7,8] The atomic parameters used[9,10,11] are listed in Table 2. Properties were extracted from the band structure using 50 *k* points in the irreducible portion of the Brillouin zone.

Results and Discussion

Electrical Resistivity. Single crystals of a tabular habit were available with the *c*-axis corresponding to the long dimension. The four-probe method measurements thus give a component of the resistivity tensor

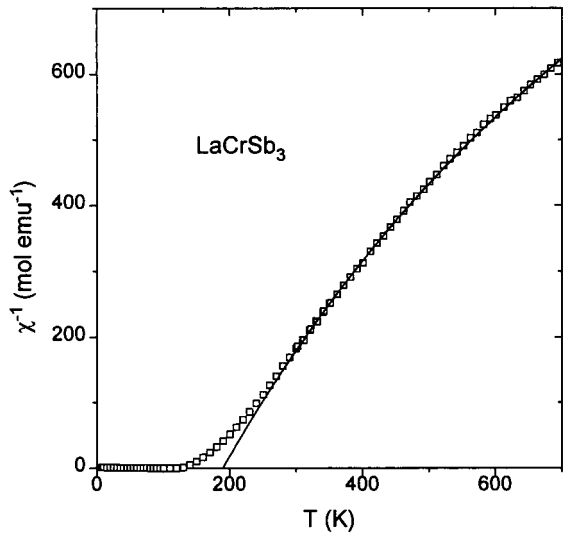

Figure 6. Inverse susceptibility for $LaCrSb_3$ over the temperature range 25−700 K.

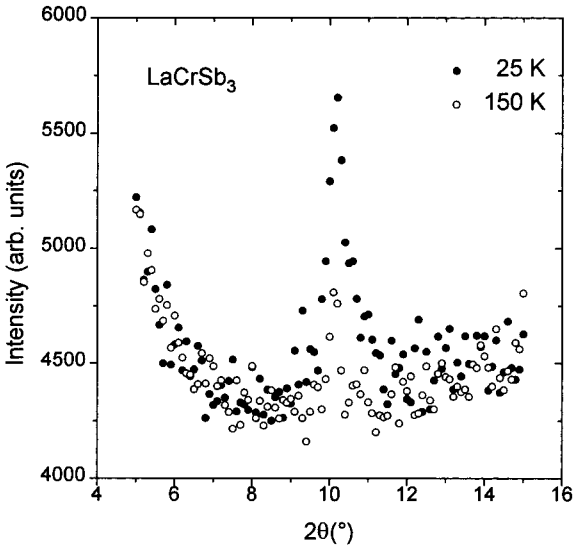

Figure 7. Neutron diffraction data for $LaCrSb_3$ near the 100 reflection at 25 and 150 K.

normal to the stacking axis *a*. Results for one crystal with dimensions 0.05 × 0.05 × 0.925 mm are shown in Figure 2. Results for other crystals were in good agreement regarding the general shape of the ρ versus *T* curve and differed in magnitude by less than 20% for the same temperature throughout the measured range. The results clearly indicate metallic behavior. Furthermore, two distinct thermal regimes exist, one from about 20 to 120−125 K, in which the ρ vs *T* curve is concave, and the second to 300 K, in which the curvature changes to convex and the increase in ρ is more gradual, approaching perhaps, a linear temperature dependence. The observed shape is typical for itinerant electron ferromagnetic materials such as $SrRuO_3$ and the pyrochlores $RE_2Mo_2O_7$, *RE* = Nd, Sm, and Gd.[12−14] The rapid decrease in the resistivity below the kink at 125

(7) Whangbo, M.-H.; Hoffmann, R. *J. Am. Chem. Soc.* **1978**, *100*, 6093.
(8) Hoffmann, R. *Solids and Surfaces: A Chemist's View of Bonding in Extended Structures*; VCH Publishers: New York, 1988.
(9) Lulei, M.; Martin, J. D.; Hoistad, L. M.; Corbett, J. D. *J. Am. Chem. Soc.* **1997**, *119*, 513.
(10) Summerville, R. H.; Hoffmann, R. *J. Am. Chem. Soc.* **1976**, *98*, 7240.
(11) Hughbanks, T.; Hoffmann, R.; Whangbo, M.-H.; Stewart, K. R.; Eisenstein, O.; Canadell, E. *J. Am. Chem. Soc.* **1982**, *104*, 3876.
(12) Bouchard, R. J.; Gillson, J. L. *Mater. Res. Bull.* **1972**, *7*, 873.
(13) Allen, P. B.; Berger, H.; Chauvet, O.; Forro, L.; Jarlborg, T.; Junod, A.; Ravez, B.; Santi, G. *Phys. Rev. B: Condens. Matter* **1996**, *53*, 4393 and references therein.
(14) Greedan, J. E.; Sato, M.; Ali, N.; Datars, W. R. *J. Solid State Chem.* **1987**, *68*, 300.

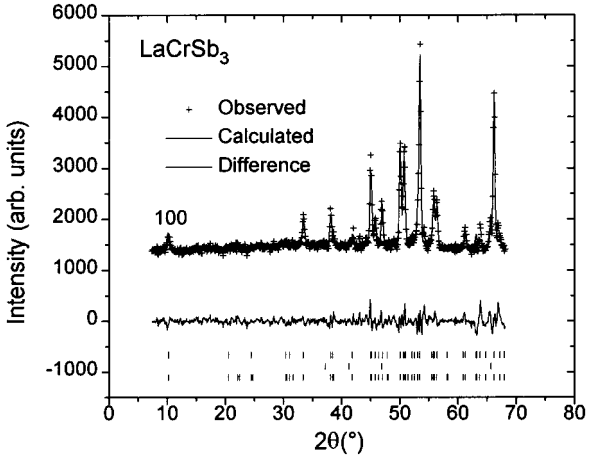

Figure 8. Rietveld refinement results for $LaCrSb_3$ at 5 K. The crosses represent the observed profile, the solid line is the fitted profile, and the difference is shown below. The three sets of vertical tic marks represent the Bragg peak positions for the $LaCrSb_3$ crystal structure (top), those for a Sb impurity phase (middle), and the magnetic peak positions (bottom). The 100 peak of largely magnetic origin is labeled.

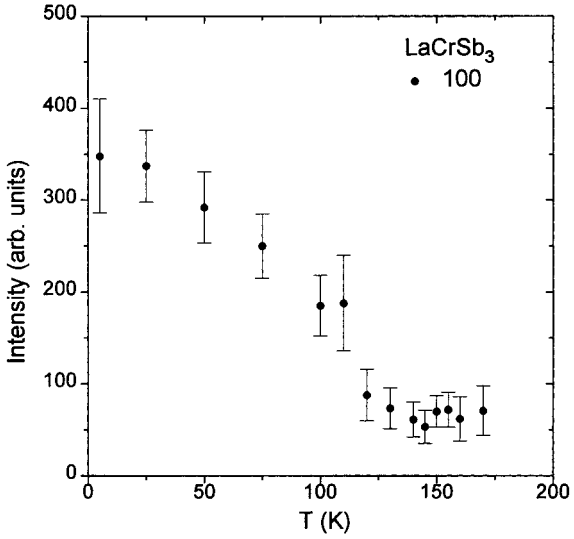

Figure 9. Temperature dependence of the 100 reflection for $LaCrSb_3$.

K is attributed to the loss of spin disorder scattering due to the onset of ferromagnetic spin order. The low-temperature data were fit to a power law of the type $\rho = \rho_0 + \alpha T^2$ (Figure 3), as has been reported for $SrRuO_3$ for example, although the exponent in the latter case was reported to be sample dependent. A plot of $d\rho/dT$ versus T (Figure 2 (inset)) shows a maximum at 120−125 K, which strongly suggests an electronic phase transition that is probably magnetic in origin in view of the evidence just presented. Unfortunately, the shape of the available crystals precludes measurements normal to the layers as a significant anisotropy might be expected.

Magnetic Measurements. The nature of the phase transition seen in the resistivity data is clarified in Figure 4, which shows the susceptibility of $LaCrSb_3$ and $-d(\chi T)/dT$ as a function of temperature. A ferromagnetic-like ordering is indicated below a T_c of 125 K. Isothermal magnetization data, shown in Figure 5, disclose a linear field dependence at 300 K, consistent with paramagnetism, and an approach to saturation at

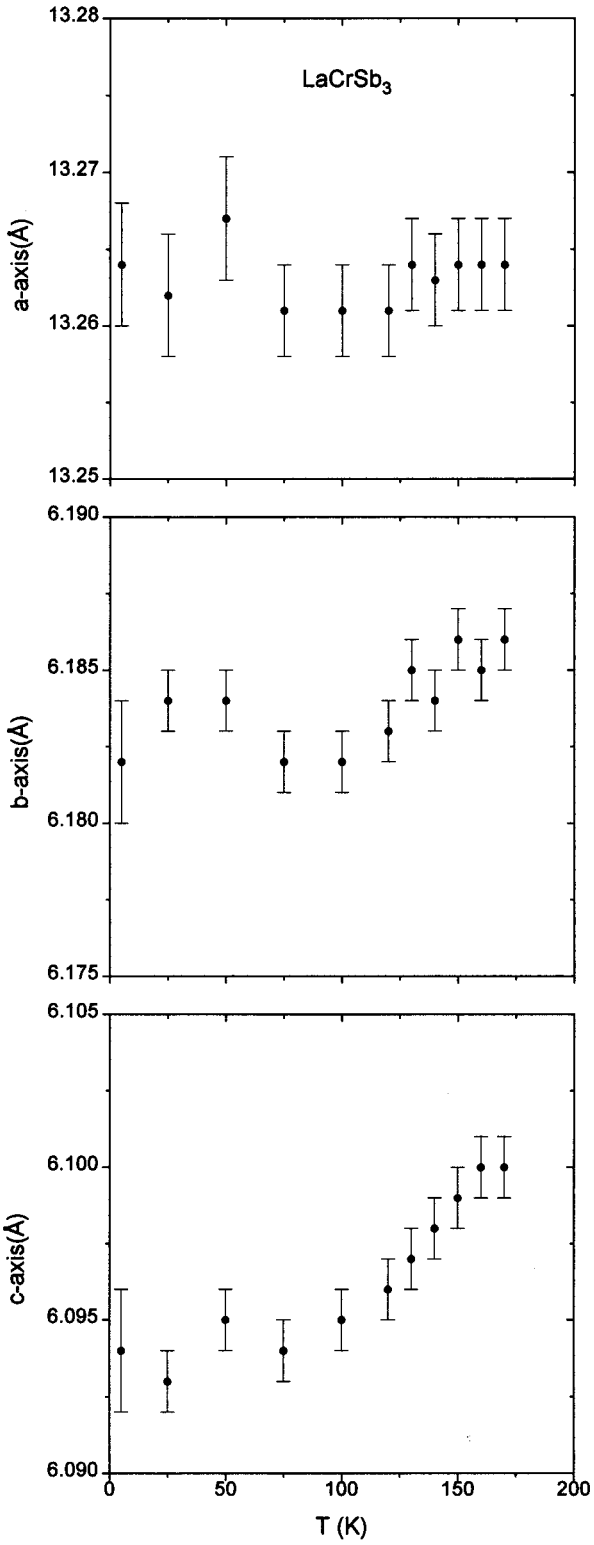

Figure 10. Temperature dependence of the unit cell constants for $LaCrSb_3$, *a*-axis (upper), *b*-axis (middle), and *c*-axis (lower).

5 K, indicative of ferromagnetism. The apparent saturation moment is about 0.8 μ_B/Cr atom at 5 T, but the weak linear dependence throughout the field regime examined makes this value somewhat uncertain. Above T_c the inverse susceptibility does not obey the Curie−Weiss law up to 700 K (Figure 6). An attempt to fit the data in the region from 300 to 700 K to a modified Curie−Weiss law by inclusion of a temperature-independent term, $\chi = C/(T - \Theta_C) + \chi_{TIP}$, yields the

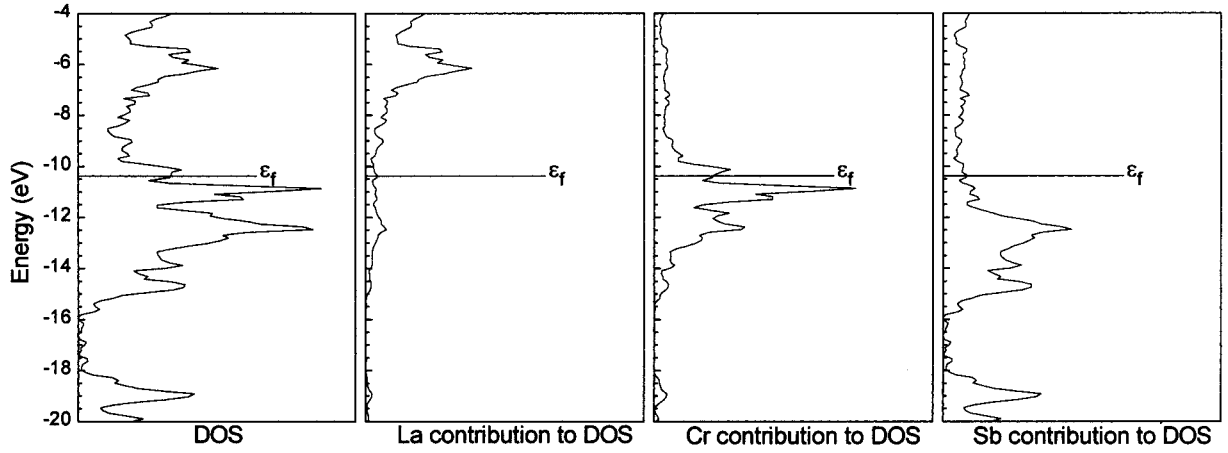

Figure 11. Total density of states for $LaCrSb_3$ (left) and the individual atomic contributions to the density of states (right).

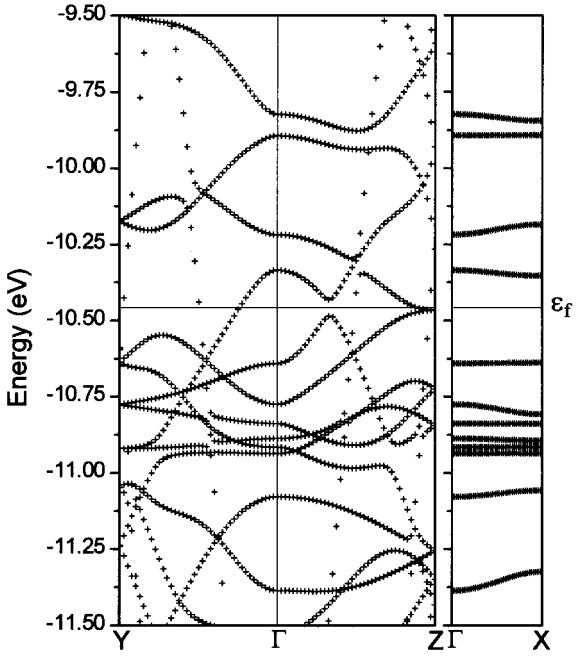

Figure 12. Band dispersion curves for $LaCrSb_3$ along the special symmetry lines ΓY, ΓZ, and ΓX.

parameters $C = 0.53$ emu K mol^{-1}, $\Theta_C = 195$ K, and $\chi_{TIP} = 5.4 \times 10^{-4}$ emu mol^{-1}. The large, positive Θ_C is consistent with ferromagnetic behavior, and the fairly large TIP term, with the metallic transport properties. Given the latter, it is unclear how to interpret the value of *C*. As mentioned earlier, Cr−Sb bond distance correlations place the Cr oxidation state intermediate between +3 and +4. The expected Curie constants for Cr^{3+} ($3d^3$) and Cr^{4+} ($3d^2$) are respectively 1.87 and 1.00, and the saturation magnetic moments are 3.0 and 2.0 μ_B. It is clear that the observed Curie constant is not consistent with any straightforward assignment of a formal oxidation state for Cr in $LaCrSb_3$. The only statement that can be made with certainty is that the non-Curie−Weiss susceptibility is consistent with an itinerant electron picture for the Cr d-electrons.

Neutron Diffraction. The bulk magnetic properties of $LaCrSb_3$ indicate ferromagnetism. Given the layered nature of the structure, it is not possible to rule out a situation in which, while the intraplanar exchange is strongly ferromagnetic, there exists a weak interplanar antiferromagnetic coupling such that a small applied field could induce a metamagnetic transition giving the appearance of bulk ferromagnetism. The true magnetic structure at zero applied field is best investigated by neutron diffraction. Data obtained at a relatively long wavelength, $\lambda = 2.3692$ Å, for temperatures above and below the apparent T_c of 125 K were examined and the observation made that only the 100 reflection is enhanced at low temperatures (Figure 7). This is not consistent with a layered antiferromagnetic structure as reflections of the type (h/2 k l) would be expected. In fact, a simulation of a simple AF structure shows a relatively strong $^1/_2$00 reflection. A fit to the diffraction profile at 5 K including the crystal structure and a ferromagnetic magnetic structure (Figure 8) demonstrates the essential correctness of this model. Refinement details for the 5 and 150 K data are collected in Table 1. The refined value for the Cr moment is 0.79(3) μ_B at 5 K with a moment direction of [010]. This is in good agreement with the saturation moment derived from the bulk polycrystalline data. The temperature dependence of the intensity of the 100 reflection (Figure 9) is consistent with a T_c of 125 K, in excellent agreement with the magnetization and resistivity data. The small residual intensity found above T_c results from the fact that 100 is an allowed reflection in *Pbcm*. These observations establish the ferromagnetic model, unequivocally.

Inspection of the refinement results shows a highly anisotropic temperature dependence of the cell constants (Figure 10). The *a*-axis (stacking direction) length is temperature independent, and the *b*-axis is nearly so. However, the dependence of the *c*-axis exhibits a change in slope at 125 K (T_c), the temperature at which magnetic ordering also occurs; this implies a strong coupling between the magnetic d-electrons and the lattice phonons.

Band Structure. As a first approximation, extended Hückel calculations were carried out. Since this method is inherently based on a one-electron model, it is not intended to provide accurate results for magnetic compounds such as $LaCrSb_3$. Rather, confirmation is sought for its gross features, namely, the metallic conductivity, the band ferromagnetism, and the extent of Cr−Cr and Sb−Sb bonding. Assuming that full electron transfer takes place, the structure of $LaCrSb_3$ partitions naturally into $La^{3+}[CrSb_3]^{3-}$. Accordingly, a band structure calculation for only the anionic $[CrSb_3]^{3-}$

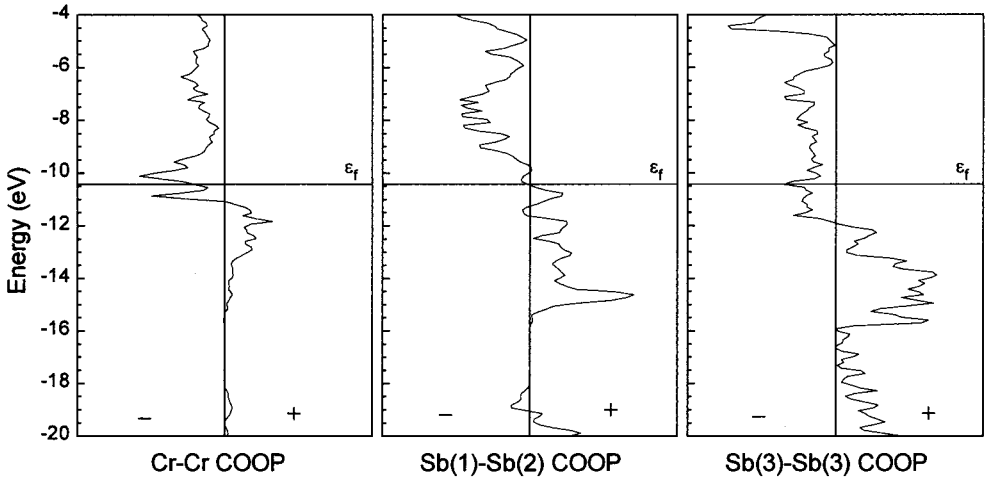

Figure 13. COOP curves for the Cr−Cr (left), Sb(1)−Sb(2) (middle), and Sb(3)−Sb(3) (right) interactions.

substructure yields results that are similar to one including the La cations as well; we report the latter results for completeness. The density of states (DOS) curve for the full 3D structure of $LaCrSb_3$ is shown in Figure 11, along with the atomic projections for each element. Figure 12 shows the band dispersion curves along the special symmetry lines ΓX (along the stacking axis of the $CrSb_2$ and Sb layers), ΓY (along the "zigzag" chains of edge-sharing $CrSb_6$ octahedra), and ΓZ (along the chains of face-sharing $CrSb_6$ octahedra).

The Fermi level ($\epsilon_f = -10.5$ eV) crosses partially filled bands in the DOS curve, consistent with metallic behavior. The La states are located well above the Fermi level, as expected for such an electropositive element, but there are also small contributions at lower energies below. Some mixing of La and Sb states may introduce a small degree of covalent character in La−Sb bonding, which is not surprising as a fully charged La^{3+} cation would be highly polarizing. Significant contributions of Cr d and Sb p states are clustered at and below the Fermi level, in the region from −9 to −16 eV. Along ΓY, bands crossed by the Fermi level are wide and their orbital compositions are primarily those of the Sb(3) atoms of the square net. Along ΓZ, bands crossed by the Fermi level are composed of orbitals from either the $CrSb_2$ layer or the Sb(3) square net. No bands are crossed, of course, along ΓX, because of the presence of the intervening layers of La cations. The interpretation is that $LaCrSb_3$ is a highly anisotropic metal in which the Sb(3) square net permits conduction in two dimensions, while the $CrSb_2$ layer conducts largely along the chains of face-sharing $CrSb_6$ octahedra.

The position of the Fermi level corresponds to nearly filling narrow, Cr-based d-bands, in a region where the DOS is relatively high. (Note also its proximity to a spike in the DOS at about −11.0 eV.) These features satisfy the general requirements for band ferromagnetism to occur—there is then the possibility that a substantial concentration of conduction electrons can populate higher energy levels with parallel spins, such that the promotion energy is still small enough to be compensated by the decrease in electron−electron repulsion. With no interactions possible along the stacking direction ΓX, the picture that emerges is one in which there is only strong ferromagnetic exchange of conduction electrons within each $CrSb_2$ layer, consistent with the neutron diffraction results.

The electronic structure is thus quite accurately described as a superposition of noninteracting $CrSb_2$ and Sb layers. After the strong Cr−Sb bonds are accounted for, Cr−Cr and Sb−Sb bonding are important secondary covalent interactions, as suggested by the COOP (crystal orbital overlap population) curves shown in Figure 13. Up to the Fermi level, all of the bonding levels are filled, but some Cr−Cr and Sb(3)−Sb(3) antibonding levels also start to fill. The cumulated overlap populations are 0.376 for Sb(1)−Sb(2) (3.175(2) Å) and 0.339 for Sb(3)−Sb(3) (3.0581(5)-3.1065(1) Å), indicating that these are significant bonding interactions. Compared with a typical overlap population of ∼0.6 for a Sb−Sb single bond of ∼2.8 Å, our earlier approximation that the ∼3.0 Å Sb−Sb bonds are of one-half bond order is fairly accurate. The ∼3.0 Å Cr−Cr interaction shows a small but nonnegligible, positive overlap population of 0.086, indicating that there is weak bonding even at this distance. The La−Sb interactions have an average overlap population of 0.190. While this implies some covalent character, it does not radically alter the bonding picture implied by the formulation $(La^{3+})(Cr^{3+})(Sb(1)^{2.5-})(Sb(2)^{2.5-})(Sb(3)^{-})$.

Acknowledgment. Financial support from the Natural Sciences and Engineering Research Council of Canada is gratefully acknowledged. We thank Dr. Mark Paetkau and Dr. John Beamish (Department of Physics, University of Alberta) for assistance in the resistivity measurements. J.E.G. thanks the NSERC for support through a Research Grant and R. Donaberger of McMaster University and I. Swainson of the NRC for assistance with the neutron diffraction experiments.

CM9803758